

## AN ADJOINT BASED METHOD FOR THE INVERSION OF THE JUNO AND CASSINI GRAVITY MEASUREMENTS INTO WIND FIELDS

ELI GALANTI

Weizmann Institute of Science, Rehovot, Israel

AND

YOHAI KASPI

Weizmann Institute of Science, Rehovot, Israel

## Abstract

During 2016-17 the Juno and Cassini spacecraft will both perform close eccentric orbits of Jupiter and Saturn, respectively, obtaining high-precision gravity measurements for these planets. This data will be used to estimate the depth of the observed surface flows on these planets. All models to date, relating the winds to the gravity field, have been in the forward direction, thus allowing only calculation of the gravity field from given wind models. However, there is a need to do the inverse problem since the new observations will be of the gravity field. Here, an inverse dynamical model is developed to relate the expected measurable gravity field, to perturbations of the density and wind fields, and therefore to the observed cloud-level winds. In order to invert the gravity field into the 3D circulation, an adjoint model is constructed for the dynamical model, thus allowing backward integration. This tool is used for examination of various scenarios, simulating cases in which the depth of the wind depends on latitude. We show that it is possible to use the gravity measurements to derive the depth of the winds, both on Jupiter and Saturn, taking into account also measurement errors. Calculating the solution uncertainties, we show that the wind depth can be determined more precisely in the low-to-midlatitudes. In addition, the gravitational moments are found to be particularly sensitive to flows at the equatorial intermediate depths. Therefore we expect that if deep winds exist on these planets they will have a measurable signature by Juno and Cassini.

## 1. INTRODUCTION

At the observed cloud-level of both Jupiter and Saturn their atmospheric dynamics are dominated by strong east-west (zonal) jet streams (Fig. 1), reaching velocities of  $140 \text{ ms}^{-1}$  on Jupiter and over  $400 \text{ ms}^{-1}$  on Saturn (Vasavada and Showman 2005). It is currently unknown how deep these jets extend (e.g., Del Genio and Barbara 2012; Li et al. 2006), and the only available direct measurements below the cloud-level are from the 1995 Galileo probe to Jupiter that found  $160 \text{ ms}^{-1}$  winds extending down at least to 22 bars at the entry point of the probe ( $6^\circ\text{N}$ ) (Atkinson et al. 1996). Addressing this question is one of the main goals of the Juno mission to Jupiter and the Cassini proximal orbits at Saturn, aiming to determine the depth extent of atmospheric circulation on these planets through precise measurements of their gravity field (Hubbard 1999; Kaspi et al. 2010). This will possibly allow answering the long lasting debate regarding the depth of the dynamics on the giant planets, and thus shed light on the mechanisms that could be driving the jets (e.g., Busse 1976; Williams 1978; Cho and Polvani 1996; Showman et al. 2006; Scott and Polvani 2007; Kaspi and Flierl 2007; Lian and Showman 2010; Liu and Schneider 2010; Liu et al. 2013).

The Juno mission was launched in 2011 and will arrive at Jupiter in 2016 equipped to perform high precision measurements of the gravity field with expected accuracy that will allow meaningful measurements up to at least  $J_{12}$  (Bolton 2005). In 2017, NASA's Cassini mission will conclude its 13 year tour of the Saturnian system, with

planned proximal orbits of Saturn obtaining the same type of data for Saturn, just before the spacecraft terminates its operation by descending into Saturn's interior. For both spacecraft the detection of the gravity signal will be done by Doppler tracking of the spacecraft trajectory.

In recent years, in anticipation of the arrival of Juno at Jupiter, several studies have looked at the effect of interior flow on the gravitational signature of the planet. To leading order, the gravity spectrum is affected by the planet's oblate shape and radial density distribution. However, on giant gas planets, since the planet is composed mainly of light elements, and have no solid surface, the relative effect of density perturbations due to their internal and atmospheric dynamics can be significant and affect the measured gravity field. Particularly, if the strong winds extend deep enough into the planets' interior, their relative effect on gravity becomes larger. This was first noted by Hubbard (1982) and later developed further by Hubbard (1999). In these studies, potential theory (the adjustment of potential surfaces under rotational and internal structure constraints) was used to show that if differential rotation on Jupiter penetrates the depth of the planet, then the resulting high-order gravity moments will be stronger than the corresponding solid-body moments. This approach was recently further developed using a more accurate concentric MacLaurin-based interior models (Hubbard 2012; Kong et al. 2012; Hubbard 2013).

These studies have allowed accurate estimation of the gravity field, but have been limited to flows following full cylindrical symmetry as these potential theory models are limited to fully barotropic systems in which the flow

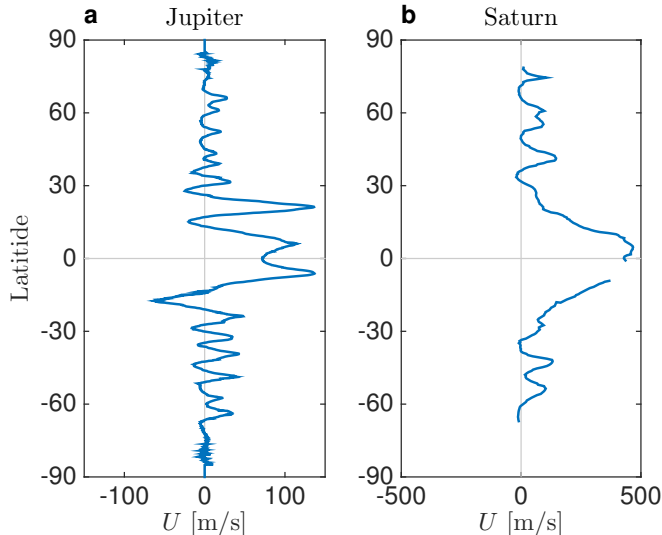


FIG. 1.— (a) Surface winds on Jupiter (Porco et al. 2003), and (b) surface winds on Saturn. Sanchez-Lavega et al. (2000)

is constant along lines parallel to the axis of rotation. A second approach proposed was using thermal wind balance models (Kaspi et al. 2010; Kaspi 2013; Kaspi et al. 2013b; Liu et al. 2013), where the gravity field resulting from any given wind field could be calculated, but these models are limited to spherical symmetry, resulting in inability to calculate the static (solid-body) gravity spectrum and neglecting the effect of the planet oblateness on the wind contribution to the gravity moments. Kong et al. (2012) calculated this effect for the case of the full barotropic flow, and found it to be small. Similarly, using a thermal-wind based model with an oblate mean state density structure we find that the effect of oblateness on the dynamical contribution to the gravity moments is small (Kaspi et al. 2013a, 2016).

Because Jupiter and Saturn are gaseous, aside from the cloud-level winds there is no apparent asymmetry between the northern and southern hemisphere. Therefore, the gravitational moments resulting from the shape and vertical structure of the planets have identically zero odd moments (Kaspi 2013). However, the observed cloud-level wind structure does have hemispherical differences, and it was shown that even if these asymmetries extend only  $O(100)$  km below the surface their contribution to the odd gravity moments is measurable (Kaspi 2013). Unlike the even moments that have a contribution both from the static density distribution and the dynamics, the odd moments are caused purely due to dynamics. Thus, any odd signal detected ( $J_3, J_5, J_7, \dots$ ) will be a sign of a dynamical contribution to the gravity signal, and this might be one of the first signals of deep dynamics that might be measured by Juno and Cassini. Using also the thermal wind approach, Liu et al. (2013) calculated the penetration depth of the winds on Jupiter with the additional assumption that the entropy gradient in the direction of the spin axis must be zero. This requirement sets the penetration depth of the winds, and they have also found that such a wind structure should be detectable by Juno and Cassini (Liu et al. 2014).

All studies to date have been only in the direction of forward modeling; thus, given a hypothetical wind structure (based on the observed surface winds and some as-

sumption regarding the penetration depth) the gravity moments are calculated via the effect of the winds on the density structure (e.g., Hubbard 1999; Kaspi et al. 2010; Liu et al. 2013; Kong et al. 2012). However, in order to analyze the gravity field that will be detected by Juno and Cassini we need to solve the inverse problem, and calculate the zonal wind profile *given* the gravity field. This causes a difficulty since a gravity field is not necessarily invertible, and a given gravity field might not have a unique corresponding wind structure. Here, we propose to address this issue using an adjoint based inverse method that will allow the investigation of the giant planet dynamics using the observed measured gravity field. This method has been used extensively in the study of oceanic and atmospheric fluid dynamics (e.g., Tziperman and Thacker 1989; Mazloff et al. 2010; Moore et al. 2011; Kalmikov and Heimbach 2014). In this study we present results based on the zonal winds only, but this method will enable to relate to the full gravity maps, not only for the zonal moments, but for the full 3D gravity fields including contributions from longitudinal variations in the wind structure and meridional winds. These variations might be detectable if the depth of these longitudinal features have a depth of at least few thousands kilometers (Parisi et al. 2016). Moreover, the adjoint model we present in this study is derived using the forward model based on the thermal wind method. However, the inversion method is more general and can be applied to more complex models (e.g., Zhang et al. 2015) or general circulation models as is often done in ocean science (e.g., Galanti et al. 2003; Mazloff et al. 2010).

In section 2 we describe the thermal wind forward method for calculating the wind induced contribution to the gravity moments, its adjoint counterpart, and the optimization procedure used to find the depth of the winds. In section 3 we discuss the results for several cases, a case with wind depth that is not varying with latitude, and a case where the winds depth on Jupiter is allowed to vary with latitude, and the same analysis applied for Saturn. We also discuss sensitivities to flow perturbations in the planet deep interior. We discuss the results and their implications for the Juno and Cassini missions in section 4.

## 2. METHODS

The relation between the density structure of the planet and the resulting gravity signature can be interpreted using the zonal gravity moments, which are defined as

$$J_n = -\frac{1}{Ma^n} \int P_n \rho r^n d^3 \mathbf{r}, \quad (1)$$

where  $M$  is the planetary mass,  $a$  is the mean planetary radius,  $P_n$  is the  $n^{\text{th}}$  Legendre polynomial and  $\rho$  is the local density (Hubbard 1984). The density can be divided into the solid-body component  $\tilde{\rho}(r, \theta)$ , and a dynamical component  $\rho'(r, \theta)$  arising from the fluid motion ( $\theta$  is latitude), so that  $\rho = \tilde{\rho} + \rho'$  (see Kaspi (2013) for more details). Similarly, in our analysis we separate the gravity moments to the static gravity signal, which is due to the static density mass distribution of the planet and is calculated using an internal structure model, and the contribution from the dynamical density perturbations due to the zonal flows. As our main goal is to determine

the penetration depth of the observed zonal flows, we take these as a given and allow a wide range of penetration depths, which are the parameters we are trying to optimize.

### 2.1. The thermal wind forward model

Starting from the observed cloud-level winds, we first need to establish the nature of the subsurface flow. Since the planet is rapidly rotating, and Coriolis accelerations are dominant over the inertial accelerations (small Rossby number), surfaces of constant angular momentum will be nearly parallel to the axis of rotation (Kaspi et al. 2009; Schneider and Liu 2009). Conservation of angular momentum then implies, to leading order, that the flow is mainly zonal, i.e., that any meridional circulation will be much weaker than the zonal flow. These zonal flows have been shown in numerical models to have a structure which is aligned with the axis of rotation, yet with wind speeds that decay with depth (Kaspi et al. 2009). Therefore, similar to Kaspi et al. (2010) we assume that the zonal wind field has the form

$$u(r, \theta) = u_0 \exp\left(\frac{r-a}{H}\right), \quad (2)$$

where  $u_0(r, \theta)$  are the observed cloud-level zonal winds extended constantly along the direction of the axis of rotation, but here we allow the e-folding decay depth of the cloud level wind,  $H(\theta)$ , to vary with latitude. This enables extra degrees of freedom in the possible structure of the winds compared to previous studies such as Kaspi et al. (2010); Kaspi (2013) and Liu et al. (2013). A latitudinal dependent decay depth can occur for several reasons, such as the internal convection extent varying with latitude (e.g., Aurnou et al. 2008), ohmic dissipation being latitudinally varying (Liu et al. 2008; Liu and Schneider 2010), moist convection having different latitudinal behavior (Lian and Showman 2010), or by different dynamics inside and outside the tangent cylinder surrounding the metallic hydrogen envelope (e.g., Heimpel and Aurnou 2007; Gastine et al. 2013; Heimpel et al. 2015). The latitude dependent  $H$  is defined as a summation over the first 20 Legendre polynomials

$$H(\theta) = \sum_{i=0}^{19} h_i P_i(\theta), \quad (3)$$

where  $h_i$  are the coefficients by which the shape of  $H(\theta)$  is determined. Such formulation allows for a solution to be found separately for different spatial scales of the winds and its resulting gravity signals. Note that when setting  $h_{i=1..19} = 0$  the depth of the winds is set to be constant with latitude. Since we expect the dynamics to be in the regime of small Rossby numbers, the flow to leading order is in geostrophic balance, and therefore thermal wind balance must hold so that

$$(2\Omega \cdot \nabla) [\tilde{\rho}\mathbf{u}] = \nabla\rho' \times \mathbf{g}_0, \quad (4)$$

where  $\Omega$  is the planetary rotation rate,  $\mathbf{u}(\mathbf{r})$  is the full 3D velocity,  $\mathbf{g}_0(r)$  is the mean gravity vector<sup>1</sup> and  $\rho'(r, \theta)$

<sup>1</sup> The gravity vector is calculated by integration of the static density  $\tilde{\rho}$ , and is therefore only a function of radius. Zhang et al. (2015) suggest a correction to this equation by adding a term as-

is the dynamical density anomaly (Pedlosky 1987; Kaspi et al. 2009). Here the thermal wind balance is written in a general form without making any assumptions on the depth of the circulation. The mean static density  $\tilde{\rho}(r)$  and  $\mathbf{g}_0(r)$  are calculated using the model of Hubbard (1999) (see also Hubbard et al. 2014). Note that, in principle, the specific choice of these background fields affects the dynamical density anomalies, however, we found that using  $\tilde{\rho}(r)$  and  $\mathbf{g}_0(r)$  from different sources hardly affects the solution of the dynamical gravity field. Therefore we consider  $\tilde{\rho}(r)$  and  $\mathbf{g}_0(r)$  as known parameters and do not try to optimize them.

Integrating the zonal component of Eq. 4 latitudinally, the dynamical density  $\rho'(r, \theta)$  can be calculated, and will depend only on the decay parameter  $H(\theta)$  and a radially depending integration constant  $\rho'_0(r)$ , which for small Rossby numbers is small compared to the solid-body radial density profile, so that  $\rho'_0 \ll \tilde{\rho}$  (Kaspi et al. 2013b). This integration constant, which physically represents a perturbation to the horizontal-mean radial density profile due to dynamics, does not contribute to the gravity field since it only depends on radius while the Legendre polynomials are only functions of latitude with a zero mean, and therefore in Eq. 1 do not contribute to the gravity moments. For this reason calculations of the gravity signal using the thermal wind method as applied here are limited to spherical geometry. Then, the dynamically induced gravity moments due to the density anomaly  $\rho'$  are

$$\Delta J_n = -\frac{1}{Ma^n} \int_0^a r'^{n+2} dr' \int_0^{2\pi} d\phi' \int_{-1}^1 P_n(\mu') \rho'(r', \mu') d\mu', \quad (5)$$

using spherical coordinates so that  $\phi$  is longitude and  $\mu = \cos\theta$ . Note that unlike the dynamical gravity moments, the static gravity moments are dominated by the oblate shape of the planet, and therefore needs to be calculated by other methods (e.g., Zharkov and Trubitsyn 1978; Kong et al. 2012; Hubbard 2012; Hubbard et al. 2014; Wisdom and Hubbard 2016).

In this study we will simulate the gravity moments, but it is important to note that resulting gravity signal itself, which can be estimated from radio tracking data, can then be calculated by taking the radial and latitudinal derivatives of the gravity potential  $V(r) = 1 - \sum_{n=2}^{\infty} \left(\frac{a}{r}\right)^n J_n P_n(\mu)$  to give the radial and latitudinal components of the anomalous gravity perturbations due to wind given by

$$\delta g_r = g_0 \sum_{n=2}^{\infty} (n+1) \lambda^n \Delta J_n P_n(\mu), \quad (6)$$

$$\delta g_\theta = g_0 \sum_{n=2}^{\infty} (1-\mu^2)^{\frac{1}{2}} \lambda^n \Delta J_n \frac{dP_n}{d\mu}, \quad (7)$$

where  $g_0$  is the mean surface gravity for the spherical planet,  $\lambda = a/(a+r_p)$ , and  $r_p$  is the local distance in the spacecraft's trajectory to the 1 bar surface. Note

sociated with the non-radial component of the gravity vector due to dynamics. However, as also shown by the same authors, for the values of decay scale heights considered here and for gravity moments with  $n > 2$  such a term is small.

that for high moments this signal increases rapidly as the spacecraft is close to periapse.

In summary, given the observed cloud-level winds, and assuming a penetration depth of the winds and the dynamical balance between them and the density structure, we can calculate the resulting gravity perturbation on the planet surface. However, the problem we need to solve is the inverse one: given the gravity measurements, what would be the  $H(\theta)$  that would best explain them. For that, we develop the adjoint model described in the next section.

## 2.2. The adjoint model

An efficient way to address the problem of determining the internal structure of the wind field, given the observations of the gravity moments  $J_n$ , a forward model such as described above, and the observed cloud-level winds, is the adjoint method. This method allows for an effective optimization of the model solution with respect to a cost function and control variables (e.g., Thacker and Long 1988; Tziperman and Thacker 1989; Tziperman 1992; Wunsch and Heimbach 2007; Mazloff et al. 2010). The adjoint method has been used extensively in geophysical fluid dynamics problems on Earth, both in the ocean (e.g., Marotzke et al. 1999; Galanti et al. 2003; Ferreira et al. 2005; Kalmikov and Heimbach 2014), and in the atmosphere (e.g., Moore et al. 2011; Blessing et al. 2014). It used for sensitivity studies as well as for optimization of parameters and data assimilation.

The cost function is the physical quantity we wish to minimize. It can be a measure of the deviation of the model solution from the observations, or simply the model solution itself. The control variables can be any parameter or model variable that has an effect on the cost function. The adjoint model is then a backward run of the derivatives of the cost function with respect to the model variables, linearized over its solution from the forward integration, with the final solution of the adjoint model being the sensitivity of the cost function with respect to the control variables. This sensitivity can be studied by itself, or be used to direct the model toward a solution that minimizes the cost function. In this study we will use the adjoint mainly for optimization, but also examine the adjoint sensitivities that enable us to evaluate the sensitivity of our solutions to the wind velocities at different depths.

The cost function is defined as the difference between the model calculated moments and those measured, and the control variable is the decay parameter  $H(\theta)$ . We define the cost function as

$$\mathcal{J} = \Delta J^T \cdot W \cdot \Delta J + \epsilon \sum_{i=0}^{19} h_i^2, \quad (8)$$

$$\Delta \mathcal{J} = J^c - J^o, \quad (9)$$

where  $J^c$  is the  $N$  size calculated model solution,  $J^o$  are the observed gravity moments, and  $W$  is a matrix of size  $N \times N$  with weights given to each moment (diagonal terms) and covariance between moments (off-diagonal terms). In general, the values of the weights are set as the inverse of the observational error covariance matrix (Finocchiaro and Iess 2010), but given the conceptual nature of this study we set for simplicity the weights to

be  $W_{ii} = 4 \times 10^{16}$  and zero elsewhere, representing simulated uncertainties of  $5 \times 10^{-9}$  (a value similar to the high moments, see more in section 3). The second term in Eq. 8 which is set to be much smaller than the first and controlled by the value of  $\epsilon$ , acts as a constraint on the optimized solution demanding that the values of  $h_i$  be as small as possible as long as they do not affect substantially the first term, thus reduce the effect of unphysical initial guess on the final solution. For example, if a certain  $h_i$  has a large value in the initial guess but has little effect on the cost function, i.e., it has a small projection on the gravitational moments, the second term acts to reduce its value. On the other hand, if that  $h_i$  has a significant projection on the gravitational moments, and therefore on the cost function, its value will be optimized. This second term should only come into play once the cost function has been substantially reduced, otherwise it will dominate the optimization process and instead of minimizing the difference between the model gravitational moments and the observed ones, the values of all  $h_i$  will be reduced regardless of their contribution to the moments. It is therefore important to keep the second term very small compared to the initial value of the cost function (at least by 2 orders of magnitude) to allow a physical optimization of the problem. With that, the value of  $\epsilon$  should also be not too small, otherwise it will have no effect on the optimization process. For each case presented here, the value of the parameter  $\epsilon$  was set according to the initial value of the cost function, to keep the necessary ratio.

Our goal is to minimize the cost function, i.e., bring the model solution closer to the observed, and therefore we need to calculate its sensitivity to changes in the decay parameter  $H(\theta)$ . For simplicity we start with a single  $H$ , so that the sensitivity is

$$\lambda(H) \equiv \frac{\partial \mathcal{J}(J_n^c)}{\partial H} \quad (10)$$

with the modeled moments formulated as a series of operators

$$J_n^c = F_1(F_2(F_3(H))), \quad (11)$$

where  $F_1$  is the solution of Eq. 5,  $F_2$  is the solution of Eq. 4, and  $F_3$  the solution of the spherical structure of the wind Eq. 2, which is a function of  $H$ .

Therefore the model Jacobian matrices for the three equations can be written in the form (e.g., Marotzke et al. 1999)

$$\lambda(H) \equiv \frac{\partial \mathcal{J}(H)}{\partial H} = \left( \frac{\partial \mathcal{J}}{\partial J_n^c} \right) \left( \frac{\partial J_n^c}{\partial \rho} \right) \left( \frac{\partial \rho}{\partial \mathbf{u}} \right) \left( \frac{\partial \mathbf{u}}{\partial H} \right). \quad (12)$$

Taking the transpose results in matrix-vector multiplications and we get

$$\lambda^T \equiv \left( \frac{\partial \mathcal{L}}{\partial H} \right)^T = \left( \frac{\partial \mathbf{u}}{\partial H} \right)^T \left( \frac{\partial \rho}{\partial \mathbf{u}} \right)^T \left( \frac{\partial J_n^c}{\partial \rho} \right)^T \left( \frac{\partial \mathcal{J}}{\partial J_n^c} \right)^T, \quad (13)$$

which is the adjoint model to be used.

The solution of the adjoint model  $\lambda^T$  is the sensitivity of the cost function to a perturbation in the control variable  $H$ . Modifying the control variable iteratively according to the adjoint solution will result in a minimization of the cost function. In the case of a latitudinal

dependent wind depth, where  $H(\theta)$  is a function of the coefficients  $h_i$ , the adjoint solution has the form

$$\lambda_i^T \equiv \left( \frac{\partial \mathcal{J}}{\partial h_i} \right)^T = \left( \frac{\partial \mathbf{H}}{\partial h_i} \right)^T \left( \frac{\partial \mathbf{u}}{\partial H} \right)^T \left( \frac{\partial \rho}{\partial \mathbf{u}} \right)^T + \left( \frac{\partial \Delta J_n^c}{\partial \rho} \right)^T \left( \frac{\partial \mathcal{J}}{\partial \Delta J_n^c} \right)^T + 2\epsilon h_i, \quad (14)$$

where  $\lambda_i^T$  is the adjoint sensitivity with respect to the  $i^{\text{th}}$  coefficient of Eq. 3. Alternatively, the adjoint sensitivities could be formulated using Lagrange multipliers (e.g., Thacker and Long 1988; Tziperman and Thacker 1989). A detailed example on how the adjoint model is derived using the Lagrange multipliers is given in Appendix ??.

The effectiveness of the adjoint method comes from its ability to provide the sensitivity to all control variables (in our case,  $h_i$ ) in a single run of the forward and backward models. Having the adjoint solution we can now proceed to construct the optimization of the model solution.

### 2.3. Optimization procedure

Once the gradient of the cost function  $\lambda$  is obtained, the control variables (either a single depth  $H$ , or coefficients  $h_i$ ) are modified so that in the next iteration the cost function will have a lower value. In the case of a single  $H$  there is only one option to change the control variable - in the direction opposite to the value of the adjoint solution. In the case of optimizing  $h_i$ , moving directly (steepest descent) is not efficient, therefore a conjugate gradient method is applied so that the direction of modifying the control variables is the optimal one (Hestenes 1980). The extent of the change is also controlled using a line search (Hestenes 1980), so that the change in the control variable does not cause the cost function to move beyond the global minimum. The global minimum is defined to be reached when each of the gravitational moments is as close to the value of the observed one as the size of the uncertainty assigned to it. Therefore, after each iteration we check the value of each element in  $\Delta J$  to see whether it is small compared to the observational uncertainty (in our case,  $5 \times 10^{-9}$ ), and if all the calculated moments are within this uncertainty the optimization is complete. At the final iteration, the Hessian matrix  $C$  (second derivative of the cost function) is calculated in order to estimate the uncertainties associated with each control variable (Tziperman and Thacker 1989). Inverting the Hessian matrix  $C$ , we get the error covariance matrix  $G$ . Finally, the cross correlated uncertainties  $G_{ij}$  are projected into the physical space of  $H$ , and used as formal bounds on the solution. Note that if the control variable is a single depth  $H$ , the size of the Hessian matrix is  $1 \times 1$ . The adjoint optimization was tested with various wind depths, and is found to be able to reach a solution within 10 to 60 iterations (see example in Figs. 2 and 3). In addition, an important criteria for the robustness of the solution is whether the minimum reached is global, i.e., would the same solution be reached if starting from different initial guesses. In order to test this we tested each of the experiments presented in this study, starting from different initial guesses and checking if the same solution is reached. An example of such a test is shown in Fig. 2, where the different

curves show the optimization process for different initial guesses. We found that in all experiments discussed in section 3 the adjoint optimization is insensitive to the choice of the initial guess - the same solution is being reached regardless of the initial guess, only the number of iterations needed might change. Therefore, we conclude that the global minimum of the problem is indeed being reached, and the method is valid for the problems presented.

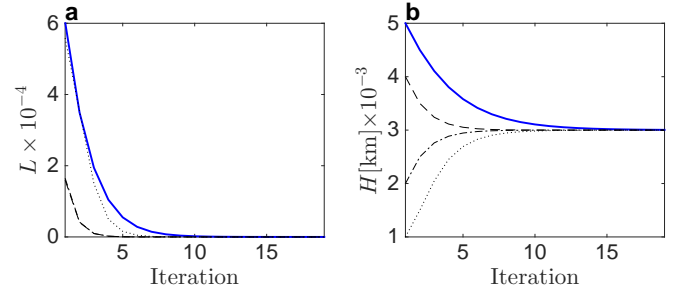


FIG. 2.— An example of the adjoint optimization. (a) the reduction of the cost function with iterations, and (b) the change in the penetration depth as function of iterations. The solid line is for the optimization starting from an initial guess of  $H = 5000$  km, while the other lines show the same optimization but with the initial guess being  $H = 4000$  km,  $H = 2000$  km and  $H = 1000$  km. In all cases, the same solution is reached. Note that due to the nonlinear nature of the problem the convergence rate is different for the cases of initial guess of  $H = 5000$  km and  $H = 1000$  km, even though they begin from the same distance from the solution. Also note that the dashed and dashed-dotted lines in (a) overlap.

## 3. RESULTS

We now show how the adjoint method is used to produce a wind structure, given the surface wind velocities and a set of gravity moments. In all cases presented below the following approach was taken: first, the forward model was run with a chosen depth of winds and the gravitational moments were calculated. These moments are then defined as the *simulation*. This solution is used to mimic the upcoming Juno or Cassini observations. In order to allow for observational errors, a uniformly distributed error with a magnitude of  $5 \times 10^{-9}$  is added to the gravity moments. This value corresponds to the average error measurement we expect for lowest order moments (Finocchiaro and Iess 2010). Second, the adjoint optimization is used to find the *solution* closest to the simulated moments, starting from an *initial guess* and then searching for the solution using the optimization procedure.

### 3.1. Inversion of the gravity signal

We start with a Jupiter case, where first for simplicity the observed winds of Jupiter are set to penetrate to the same depth in all latitudes. Therefore the adjoint optimization is trying to minimize the cost function with respect to a single depth  $H$ . The simulation is done with  $H = 3000$  km, and the initial guess was set to  $H = 5000$  km. The progression of the adjoint optimization is shown in Fig. 2 (solid lines). It can be seen that the within 5 iterations the cost function value is reduced by an order of magnitude, and the calculated wind depth is getting closer to the simulated one. The gravitational moments for the simulation, initial guess, and

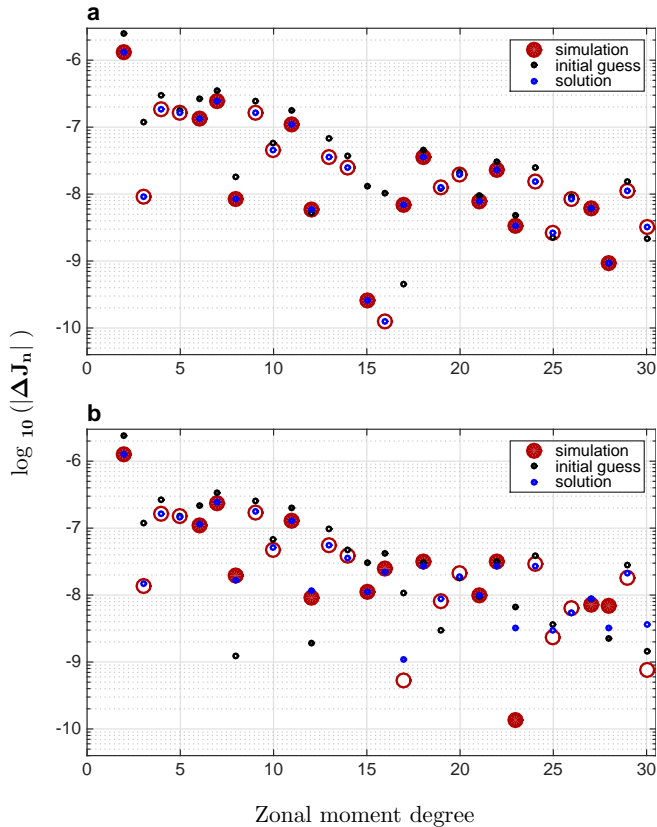


FIG. 3.— The Jupiter gravitational moments for (a) a case with no errors in the simulated moments, and (b) a case with random errors. Shown are the simulation (red), initial guess (black), and solution (blue). Filled (open) circles denote positive (negative) values.

solution are shown in Fig. 3 for a case without errors in the simulated moments (panel a) and for a case with errors (panel b). While in the former case the moments reach a perfect fit to the simulation, in the latter case the lower moments are fitted well and the higher moments are less so, since the errors applied to the simulation have a relatively larger effect on the higher moments which are smaller.

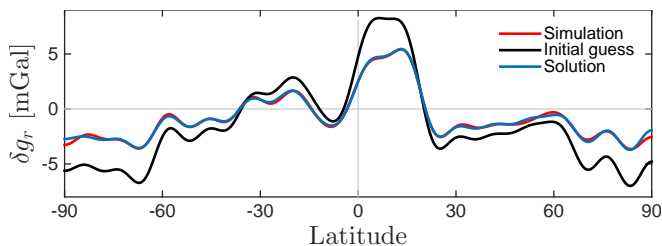


FIG. 4.— A case with simulated  $H = 3000$  km and the initial guess  $H = 5000$  km. Shown are the radial component of the gravitational anomalies (in mGals) as function of latitude, for the simulation (red), initial guess (black), and solution (blue).

The gravitational moments can be transformed into the actual latitudinal dependent gravity anomalies (Eq. 6). The radial component of these anomalies, calculated at the planet’s 1 bar level, are shown in Fig. 4, for the adjoint solution, together with the simulation and initial guess. Note that as a result of the complex sur-

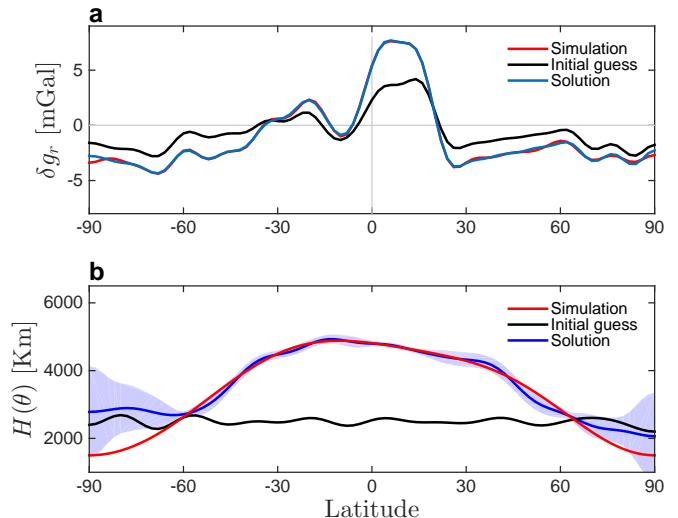


FIG. 5.— A case with latitudinal depended decay depth  $H(\theta)$ . (a) The gravitational anomalies (in mGals) as function of latitude, and (b) the depth of the winds. Shown are the simulation (red), initial guess (black), and solution (blue). For the solution of the wind depth, also shown are the associated uncertainties (blue shading).

face wind structure (Fig. 1), even with a single  $H$  the resulting gravity field has a pronounced asymmetry between the Northern and Southern hemispheres. While the initial guess differs considerably from the simulation, the solution matches well the simulation. The difference between the simulation and the solution is a result of the errors we apply to the simulation. In a case with no random errors the solution is identical to the simulation (not shown). Given the good agreement between the adjoint solution and the simulation, it is clear that most of the gravity signal is contained in the lower moments. Note that the differences in the moments (Fig. 3) have only minor effect on the actual gravity field; therefore, for the next more complicated cases, we show the gravity field and not the gravitational moments.

Next, the winds penetration depth is allowed to vary with latitude. In this case, the adjoint optimization is trying to minimize the cost function with respect to the set of coefficients  $h_i$ . The simulation was done with an  $H(\theta)$  that is deeper at the equator and shallower toward the poles, representing possibly deeper dynamics outside of the tangent cylinder (Aurnou et al. 2007), where drag might be playing a lesser role (Liu and Schneider 2010). The simulation  $H(\theta)$  has an asymmetry between the hemispheres, and the initial guess was chosen to reflect a complex dependence on latitude (Fig. 5b). The adjoint solution over most latitudes (see below) is in good agreement with the simulation, in both the gravity anomalies (Fig. 5a) and the depth of the winds (Fig. 5b).

The adjoint model also gives us the ability to rigorously estimate the uncertainty associated with the solution. This is done by calculating the Hessian matrix and from that, the error covariance matrix (Fig. 6a and Fig. 6b, respectively). The Hessian matrix gives an estimate to the sensitivity of the cost function to cross perturbations in the control variables; the higher the value, the better is our ability to determine the values of these parameters. Inverting the Hessian matrix reveals the covariance of the uncertainties associated with each control



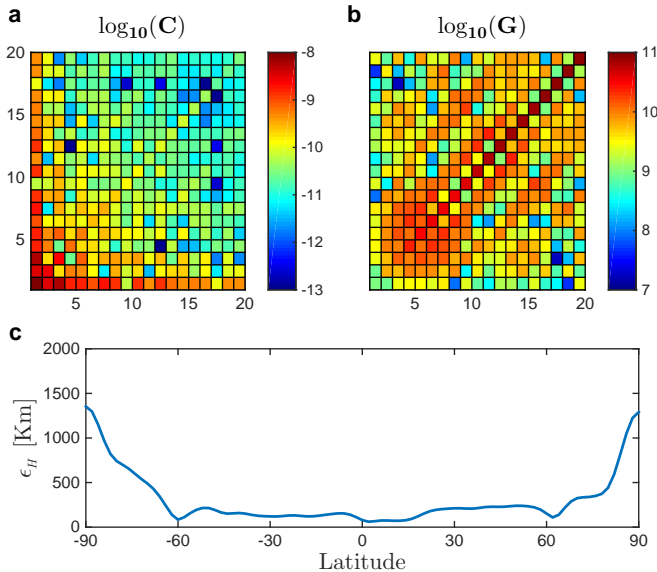


FIG. 6.— (a) Hessian matrix associated with the adjoint solution. (b) The error covariance matrix. (c) The uncertainties in the solution for the depth of the winds, as calculated from the diagonal of the error covariance.

variable (Fig. 6b). The highest uncertainties are in the diagonal terms of the higher coefficients, meaning that the coefficients are not affecting much each other, and that most of the uncertainties are in the spatially highly variable features (higher moments). In order to further verify this, the covariance matrix can be used to calculate the uncertainty in  $H$  at each latitude using

$$\epsilon_H(\theta) = \sqrt{\sum P_i(\theta)P_j(\theta)G_{ij}} \quad (15)$$

where  $G_{ij}$  are the cross correlation between the coefficients  $h_i$  and  $h_j$ , and  $P_i(\theta)$  is the Legendre polynomial at latitude  $\theta$ . The uncertainty in  $H$  (Fig. 6c), is found to be largest near the poles since this is where the winds are weakest. This uncertainty is plotted also in Fig. 6b to illustrate the usefulness of the solution for  $H$ . It is clear that where the uncertainty in  $H$  is small, the solution matches well the simulation (low latitudes), and where the uncertainty is large the solution deviates considerably from the simulation (high latitudes). This has implications for the expected usefulness of the upcoming gravitational measurements by Juno and Cassini in determining the depth of the winds on both Jupiter and Saturn. Even in a case where the uncertainties of the measured gravity field is very small, due to the weak wind close to the poles it will not be possible to determine with certainty the depth of the flow in the polar regions. Moreover, the planned periapses of the orbit of both Juno and Cassini are at low latitudes, meaning that the sensitivity to higher latitude induced signals will be smaller (Finocchiaro and Iess 2010; Finocchiaro 2013).

Next, we repeat the experiment for Saturn. The main difference between the planets, aside from the different physical parameters, is in the surface wind pattern (Sanchez-Lavega et al. 2000, 2007; Garcia-Melendo et al. 2011). While on Jupiter the winds vary considerably with latitude, on Saturn the much stronger winds have a simpler latitudinal pattern (Fig. 1). As in the Jupiter case, the simulation was done with  $H$  that is deeper

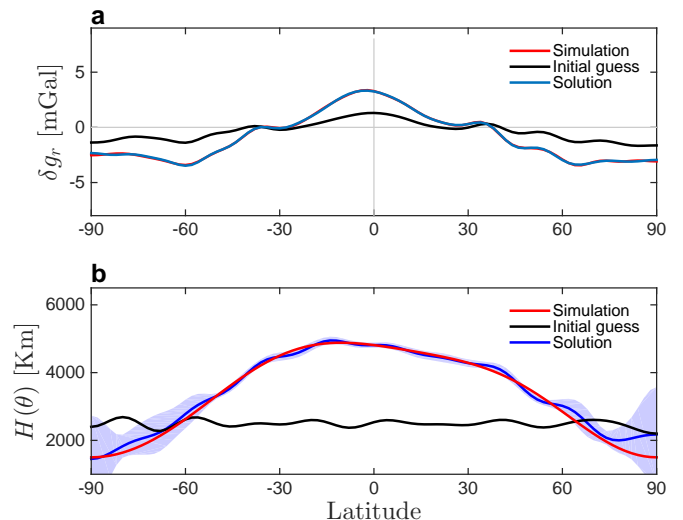


FIG. 7.— (a) The Saturn gravitational anomalies (in mGals) as function of latitude, and (b) the depth of the winds. Shown are the simulation (red), initial guess (black), and solution (blue). For the solution of the wind depth, also shown are the associated uncertainties (blue shadow).

at the equator and shallower toward the poles, with an asymmetry between the hemispheres; the initial guess was chosen to reflect a complex dependence on latitude (Fig. 7b). Since the shape of the surface winds are much different in the Saturn case, the resulting gravity anomalies are also very different (Fig. 7a). Still, similarly to the Jupiter case, the solution matches closely the simulation in the low latitudes and less so closer to the poles. This characteristic is evident in the associated uncertainties, shown in Fig. 7b as the shaded area around the solution.

### 3.2. Changing the physical assumptions

So far we used the same physical assumptions in both the model used for calculating the ‘simulation’ and the model used to find the ‘solution’. However, a valid question is how well would the adjoint optimization work when the model used to find the solution is different from the one used for generating the simulation - in the reality we should expect that any model used to interpret Juno observations will lack some of the physics embedded in the observations.

In order to get insight on the matter, we examine two cases in which the model used for optimization differs from that used for the simulation. First, we set the ‘simulation’ with the depth of the wind being constant with latitude, and ask the optimization to look for a depth that varies with latitude (Fig. 8). The simulation was done with  $H = 4000$  km, the initial guess was set with depth of winds that vary between 3000 km near the equator and 1000 km near the poles. The optimized solution follows closely the simulated depth, aside from the polar regions where it deviate by about 1000 km (as expected from its uncertainties). This experiment challenges the optimization more than the previous ones, but is still within the framework of the physical model used for both simulation and optimization, since we can view the simulation as done with latitude varying depth set with Eq. 3 with  $h_0 = 4000$  km and  $h_{1-19} = 0$ .

A more challenging setup can be done by generating the simulation with a latitude varying depth and looking

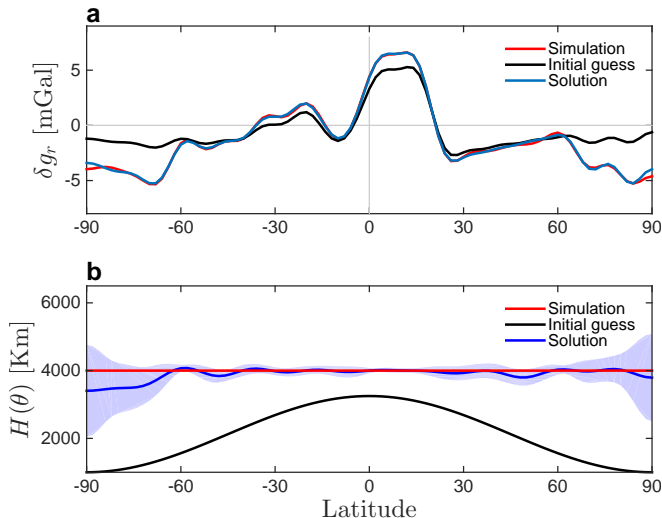


FIG. 8.— A case where the simulated wind depth is constant with latitude and the solution varies with latitude. (a) Jupiter gravitational anomalies (in mGals) as function of latitude, and (b) the depth of the winds. Shown are the simulation (red), initial guess (black), and solution (blue). For the solution of the wind depth, also shown are the associated uncertainties (blue shadow).

for a solution in which the depth of the wind is assumed constant with latitude. In such a case we can expect that the simulated solution could not be reached, since the physical model used in the optimization lacks some of the physics used in the simulation. We set the experiment with the simulation based on the same depth distribution as in the previous section, and set the initial guess to be  $H = 2000$  km (Fig. 9). As expected, it can be seen that the solution  $H = 4327$  km does not match the simulated one, yet it is in the proximity of the wind depth in the equatorial region. Moreover, looking at the actual gravity field (Fig. 9a), the solution captures most of the signal contained in the simulation, especially in the low and mid-latitudes.

The two experiments discussed here show that the adjoint method can deal with cases in which the physical assumptions regarding the depth of the wind used in the optimization differ from those used in the simulation. In the next section we discuss the sensitivity of the solution to deep flow patterns, an additional complication.

### 3.3. Sensitivity to deep wind patterns

Aside from the question of how deep the cloud-level winds penetrate, it might also be the case that a different structure of flow exists in the interior, that does not have any signature at the observed cloud-level wind. As deeper levels have more mass, it is possible that the measured gravity signal will come from these levels (Galanti and Kaspi 2015). As long as this flow structure will be large scale it will also likely be geostrophic and therefore in thermal wind balance, with an associated density modulation that will affect the gravity field. Using the adjoint method we can get an estimate on the sensitivity of the cost function to perturbations in the 2-dimensional wind field, regardless of the surface winds. In fact this can be also done in 3D, using the Tesseral moments (Parisi et al. 2016), but as the aim of this study is to present this method, we keep here the analysis simple with just the 2D (zonally averaged) wind fields. To perform this

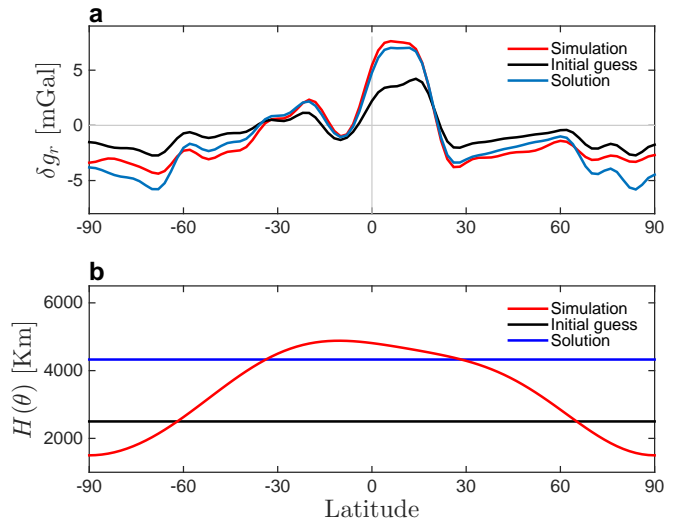


FIG. 9.— A case where the simulated wind depth varies with latitude but the solution has a constant depth. (a) Jupiter gravitational anomalies (in mGals) as function of latitude, and (b) the depth of the winds. Shown are the simulation (red), initial guess (black), and solution (blue).

estimate, the forward model was run with a wind depth of 5000 km (this choice does not affect the solution, aside from some minor nonlinear contributions). Defining the cost function to be the sum of the square of the gravitational moments

$$\mathcal{J} = \sum_n W_n (J_n^c)^2, \quad (16)$$

the adjoint model is integrated to produce the adjoint sensitivities, which are the sensitivity of the cost function to any of the model prognostic variables. In our case they include the gravitational moments, the density perturbations, the wind structure, and the depth parameter (see Eq. 13). The value of the sensitivities is the change in the cost function expected when perturbing the variable with a unit change.

We then save the adjoint variables of both the density and wind,

$$\lambda_\rho(z, \theta) \equiv \left( \frac{\partial \mathcal{J}^c}{\partial \rho} \right)^T \left( \frac{\partial \mathcal{J}}{\partial \Delta J^c} \right)^T, \\ \lambda_U(z, \theta) \equiv \left( \frac{\partial \rho}{\partial \mathbf{u}} \right)^T \left( \frac{\partial \mathcal{J}^c}{\partial \rho} \right)^T \left( \frac{\partial \mathcal{J}}{\partial J^c} \right)^T, \quad (17)$$

that are a function of latitude and depth. The adjoint solution for the sensitivity to the density and wind is specific to the model's numerical structure in general, and to the grid structure in particular. Given that the grid in the model is not regular, i.e., the size of the grid box changes with depth, the adjoint solution needs to be normalized by the size of the grid box in order to show the physical sensitivity. Figure 10 shows the normalized sensitivities to density perturbations and wind perturbations. While the sensitivities to the density mostly bears the shape of  $J_2$ , and are highest close to the surface (due to the strong dependence of the gravitational moments on the distance from the surface), the sensitivities to the zonal velocity show a different structure. There exist a single pattern of positive sensitivities, located close to the equator, with the maximum around



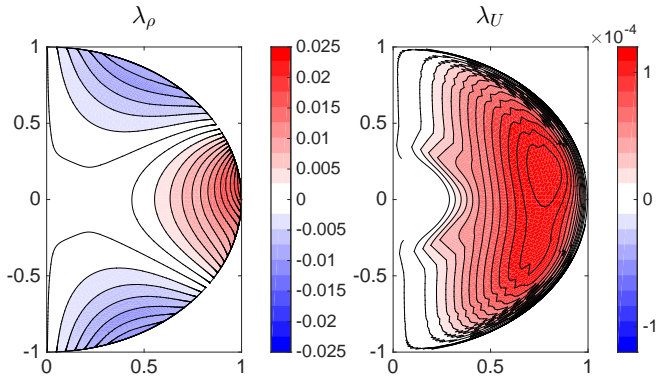


FIG. 10.— Sensitivity of the cost function to perturbations in  $\rho$  (left) and  $U$  (right).

a depth of 10,000 km from the surface. The sensitivities decay gradually toward high latitudes. This is due to the nature of the thermal wind balance, in which the vertical gradient of the density is a function of the latitudinal gradient of the wind, so that a wind perturbation at a certain depth will imply a density perturbation from that depth to the surface. This implies that the highest sensitivities to deep winds, if they exist, will be to winds at the range of  $\sim 10,000$  km below the cloud-level and limited to low latitudes. This issue, of the possibility that deep flows exist separately from the surface wind and their affect on the gravity field, needs to be further examined in future studies.

#### 4. DISCUSSION AND CONCLUSION

Modern observations of the gas giants since the 1970s have allowed studying these planets in great detail, particularly regarding processes at their cloud-level. Yet, much of the processes controlling the levels below have remained unknown mainly due to lack of observational data. This will likely change in the coming few years as the upcoming Juno mission and Cassini proximal orbits bring the possibility of investigating in detail the sub-cloud levels with several different instruments. Particularly, Radio measurements will provide high precision gravity soundings, i.e., data that can be used to estimate the depth of the observed surface flows on these planets. All models to date, relating the winds to the gravity field, have been in the forward direction, thus allowing only a calculation of the gravity field from a given wind model. Here, we propose a method to solve the inverse problem of deriving the depth of the winds from the gravity data. We use an adjoint based inverse dynamical model to relate the expected measurable gravity field, to perturbations of the density and wind fields, and therefore to the observed cloud-level winds. In order to invert the gravity field to be measured by Juno and Cassini into the circulation, an adjoint model is constructed for the dynamical model, thus allowing backward integration of the thermal wind model.

The thermal wind method allows perhaps the simplest relation between the flow velocity and the dynamically balanced density gradients, which can be then related to the gravity field. Therefore, we have applied the adjoint method to the thermal wind model; however, the methodology presented here is not specific to this model and could be used to study and optimize any type of model, ranging from simple conceptual models to complex general circulation models (e.g., Marotzke et al. 1999; Galanti et al. 2003; Mazloff et al. 2010). In any such model the adjoint method will allow backward calculation of the flow field that best matches the measured gravity field. Models with more complex physics will allow the inclusion of processes not taken into account here such as magnetic effects, internal convection etc. Nonetheless, as long as the large scale motion on these planets is controlled to leading order by the rotation of the planet, even models containing more physical processes would be to leading order in thermal wind balance. Therefore, this analysis captures the leading order dynamical balance between the gravity and the winds. More sophisticated wind structures with more complex depth and latitudinal dependencies, and weaker coupling to the cloud-level wind can also be considered.

This tool proves to be useful for various scenarios, simulating cases in which the depth of the wind is constant, or varies with latitude. We show that it is possible to use the gravity measurements to derive the depth of the winds, both on Jupiter and Saturn, taking into account also measurement errors. We find that due to the winds on both planets being much stronger in the equatorial regions, the model solutions are better determined in the low to mid-latitudes, while the depth of the winds close to the poles cannot be determined with good accuracy. Comparing Jupiter and Saturn, it is found that the latitudinal shape of the winds affects considerably the gravity field. The adjoint method also enables showing which regions of the planet are most impactful on the gravity field. We find that the gravitational moments are most sensitive to winds at depths of around 10,000 km, especially at the equatorial region, but the signature of deep flows will appear in the gravity field even if the flows are much shallower. Therefore, if deep winds exist on these planets, they will likely leave a measurable signature in the upcoming measurements.

**Acknowledgments:** We thank the Juno science team and Eli Tziperman for useful discussions. This research has been supported by the Israeli ministry of Science under grants (3-11481 and 45-851-641), and the Helen Kimmel Center for Planetary Science at the Weizmann Institute of Science.

#### APPENDIX

##### AN EXAMPLE ON THE DERIVATION OF THE ADJOINT MODEL

In order to give a better understanding of the adjoint method we illustrate the derivation of the adjoint equations for a simple case. The same principle could be applied to any set of partial differential equations (see another example in Tziperman and Thacker 1989). Consider a simple one-dimensional advection-diffusion equation in steady state for

a tracer  $c(x)$

$$uc_x = kc_{xx}, \quad (\text{A1})$$

where the parameters we wish to optimize are  $u$  and  $k$  (the parameters in this example are equivalent to depth of the wind in our experiments, and the tracer is equivalent to the density or velocity fields). We set the two boundary conditions as

$$\begin{aligned} uc - kc_x|_{x=0} &= F_0, \\ uc - kc_x|_{x=L} &= F_L. \end{aligned} \quad (\text{A2})$$

The cost function is set to be the difference between the calculated tracer  $c$  and the observed tracer  $c^{\text{obs}}$

$$\mathcal{J} = \frac{1}{2} \int_0^L (c(x) - c^{\text{obs}}(x))^2 dx.$$

Next, we define a Lagrange function to include the constraints due to the dynamical equation (A1)

$$\mathcal{L} = \mathcal{J} + \int_0^L \lambda(uc_x - kc_{xx})dx, \quad (\text{A3})$$

where  $\lambda$  is the Lagrange multiplier that will turn out to be the adjoint variable for the tracer  $c$ . As the second term is identically zero, the values of  $\mathcal{L}$  and  $\mathcal{J}$  are equal. The minimum of the cost function  $\mathcal{J}$  (model solution) is reached when the Lagrange function  $\mathcal{L}$  has an extremum (zero derivative). Consider an arbitrary variation in the function  $c$ ,

$$\delta\mathcal{L} = \mathcal{L}(c + \delta c) - \mathcal{L}(c) = \int_0^L (c(x) - c^{\text{obs}}(x)) \delta c dx + \int_0^L \lambda(u\delta c_x - k\delta c_{xx})dx, \quad (\text{A4})$$

where  $\delta c$  is an infinitesimally small arbitrary function in  $x$ , aside from the boundaries where it must conform to the boundary conditions (see details below). Applying integration by parts we get

$$\begin{aligned} \delta\mathcal{L} &= \int_0^L [c(x) - c^{\text{obs}}(x) - (u\lambda_x + k\lambda_{xx})] \delta c dx \\ &+ \lambda [u\delta c - k\delta c_x]_{x=0}^L \\ &+ \delta c [k\lambda_x]_{x=0}^L. \end{aligned} \quad (\text{A5})$$

We need now two conditions under which  $\delta\mathcal{L}$  is zero. The second line in Eq. A5 has exactly the formulation of the boundary conditions stated above but for the variation  $\delta c$ . Since the boundary conditions should not change with variations in  $c$ , this term is zero by definition. Next, we can demand that the third line vanishes for any  $\delta c$ , i.e., that the boundary conditions for the adjoint variable  $\lambda$  are  $[k\lambda_x]_{x=0}^L = 0$ . We can do so because  $\lambda$  is not a physical variable so its boundary conditions could be set to fit the requirement on  $\mathcal{L}$ . Finally, we demand that  $\delta\mathcal{L}$  is zero for any function  $\delta c$ , therefore the integrand in the first line of Eq. A5 must vanish, which gives an equation for the adjoint variable  $\lambda$

$$u\lambda_x + k\lambda_{xx} = c(x) - c^{\text{obs}}(x). \quad (\text{A6})$$

Finally, once we have the formulation for the adjoint variable  $\lambda$ , we can optimize the cost function with respect to the parameters  $u$  and  $k$ . The derivative of the cost function with respect to these two parameters could be easily found by differentiation of Eq. A3 with respect to the two variables, so that

$$\frac{\partial\mathcal{L}}{\partial u} = \int_0^L \lambda c_x dx, \quad \frac{\partial\mathcal{L}}{\partial k} = - \int_0^L \lambda c_{xx} dx. \quad (\text{A7})$$

Thus, calculating  $\lambda$  (the sensitivity of the cost function with respect to the tracer  $c$ ), and then integrating using Eq. A7, we can find the gradient of the cost function with respect to the control variables, i.e., the direction in which those parameters should be changed in order to reach the minimum of the cost function. Note that the control variables should be modified in the direction opposite to the adjoint solution. Given that solving this example, and the actual model described in this study, needs to be done numerically, it is important that the adjoint model is actually derived from the finite difference formulation of the forward model, and not from the analytical version. The adjoint of the finite difference was shown to be more accurate than the finite difference of the adjoint (Sirkes and Tziperman 1997).

#### REFERENCES

- Atkinson, D. H., Pollack, J. B., and Seiff, A. (1996). Galileo doppler measurements of the deep zonal winds at Jupiter. *Science*, 272:842–843.
- Aurnou, J., Heimpel, M., Allen, L., King, E., and Wicht, J. (2008). Convective heat transfer and the pattern of thermal emission on the gas giants. *Geophysical Journal International*, 173:793–801.

- Aurnou, J., Heimpel, M., and Wicht, J. (2007). The effects of vigorous mixing in a convective model of zonal flow on the ice giants. *Icarus*, 190:110–126.
- Blessing, S., Kaminski, T., Lunkeit, F., Matei, I., Giering, R., Köhl, A., Scholze, M., Herrmann, P., Fraedrich, K., and Stammer, D. (2014). Testing variational estimation of process parameters and initial conditions of an earth system model. *Tellus A*, 66.
- Bolton, S. J. (2005). Juno final concept study report. Technical Report AO-03-OSS-03, New Frontiers, NASA.
- Busse, F. H. (1976). A simple model of convection in the Jovian atmosphere. *Icarus*, 29:255–260.
- Cho, J. and Polvani, L. M. (1996). The formation of jets and vortices from freely-evolving shallow water turbulence on the surface of a sphere. *Phys. of Fluids*, 8:1531–1552.
- Del Genio, A. and Barbara, J. (2012). Constraints on saturn’s tropospheric general circulation from cassini {ISS} images. *Icarus*, 219(2):689 – 700.
- Ferreira, D., Marshall, J., and Heimbach, P. (2005). Estimating eddy stresses by fitting dynamics to observations using a residual-mean ocean circulation model and its adjoint. *J. Phys. Oceanogr.*, 35:1891.
- Finocchiaro, S. (2013). Numerical simulations of the Juno gravity experiment. Ph.D. thesis. *Pubblicazioni Aperte Digitali della Sapienza, code 1889*.
- Finocchiaro, S. and Iess, L. (2010). Numerical simulations of the gravity science experiment of the Juno mission to Jupiter. In *Spaceflight mechanics*, volume 136, pages 1417–1426. Amer. Astro. Soc.
- Galanti, E. and Kaspi, Y. (2015). Deciphering Jupiter’s complex flow dynamics using the upcoming Juno gravity measurements and an adjoint based dynamical model. In *AAS/ 47th Division for Planetary Sciences Meeting Abstracts. 403.08*.
- Galanti, E., Tziperman, E., Harrison, M., Rosati, A., and Sirkes, Z. (2003). A study of ENSO prediction using a hybrid coupled model and the adjoint method for data assimilation. *Mon. Weath. Rev.*, 131:2748.
- Garcia-Melendo, E., Perez-Hoyos, S., Sanchez-Lavega, A., and Hueso, R. (2011). Saturn’s zonal wind profile in 2004–2009 from Cassini ISS images and its long-term variability. *Icarus*, 215(1):62–74.
- Gastine, T., Wicht, J., and Aurnou, J. M. (2013). Zonal flow regimes in rotating anelastic spherical shells: An application to giant planets. *Icarus*, 225:156–172.
- Heimpel, M. and Aurnou, J. (2007). Turbulent convection in rapidly rotating spherical shells: A model for equatorial and high latitude jets on Jupiter and Saturn. *Icarus*, 187:540–557.
- Heimpel, M., Gastine, T., and Wicht, J. (2015). Simulation of deep-seated zonal jets and shallow vortices in gas giant atmospheres. *Nature Geosci.*, advance online publication.
- Hestenes, M. (1980). *Conjugate direction methods in optimization*.
- Hubbard, W. (1982). Effects Of Differential Rotations On The Gravitational Figures Of Jupiter And Saturn. *Icarus*, 52(3):509–515.
- Hubbard, W. B. (1984). *Planetary interiors*. New York, Van Nostrand Reinhold Co., 1984, 343 p.
- Hubbard, W. B. (1999). Note: Gravitational signature of Jupiter’s deep zonal flows. *Icarus*, 137:357–359.
- Hubbard, W. B. (2012). High-precision Maclaurin-based models of rotating liquid planets. *Astrophys. J. Lett.*, 756:L15.
- Hubbard, W. B. (2013). Conventric maclaurian spheroid models of rotating liquid planets. *Astrophys. J.*, 768(1).
- Hubbard, W. B., Schubert, G., Kong, D., and Zhang, K. (2014). On the convergence of the theory of figures. *Icarus*, 242:138–141.
- Kalmikov, A. and Heimbach, P. (2014). A hessian-based method for uncertainty quantification in global ocean state estimation. *SIAM Journal on Scientific Computing*, 36:S267–95.
- Kaspi, Y. (2013). Inferring the depth of the zonal jets on Jupiter and Saturn from odd gravity harmonics. *Geophys. Res. Lett.*, 40:676–680.
- Kaspi, Y., Davighi, J., Galanti, E., and Hubbard, W. (2013a). Estimating the depth of the zonal jet streams on Jupiter and Saturn through inversion of gravity measurements by Juno and Cassin. *AGU Fall Meeting Abstracts*.
- Kaspi, Y., Davighi, J. E., Galanti, E., and Hubbard, W. B. (2016). The gravity signature of atmospheric dynamics on giant planets: comparison between the potential theory and thermal wind approaches. *Icarus*. under revision.
- Kaspi, Y. and Flierl, G. R. (2007). Formation of jets by baroclinic instability on gas planet atmospheres. *J. Atmos. Sci.*, 64:3177–3194.
- Kaspi, Y., Flierl, G. R., and Showman, A. P. (2009). The deep wind structure of the giant planets: Results from an anelastic general circulation model. *Icarus*, 202:525–542.
- Kaspi, Y., Hubbard, W. B., Showman, A. P., and Flierl, G. R. (2010). Gravitational signature of Jupiter’s internal dynamics. *Geophys. Res. Lett.*, 37:L01204.
- Kaspi, Y., Showman, A. P., Hubbard, W. B., Aharonson, O., and Helled, R. (2013b). Atmospheric confinement of jet streams on Uranus and Neptune. *Nature*, 497:344–347.
- Kong, D., Zhang, K., and Schubert, G. (2012). On the variation of zonal gravity coefficients of a giant planet caused by its deep zonal flows. 748.
- Li, L., Ingersoll, A., Vasavada, A., Simon-Miller, A., Del Genio, A., Ewald, S., Porco, C., and West, R. (2006). Vertical wind shear on jupiter from cassini images. *Journal of Geophysical Research: Planets*, 111(E4):n/a–n/a.
- Lian, Y. and Showman, A. P. (2010). Generation of equatorial jets by large-scale latent heating on the giant planets. *Icarus*, 207:373–393.
- Liu, J., Goldreich, P. M., and Stevenson, D. J. (2008). Constraints on deep-seated zonal winds inside Jupiter and Saturn. *Icarus*, 196:653–664.
- Liu, J. and Schneider, T. (2010). Mechanisms of jet formation on the giant planets. *J. Atmos. Sci.*, 67:3652–3672.
- Liu, J., Schneider, T., and Fletcher, L. N. (2014). Constraining the depth of saturn’s zonal winds by measuring thermal and gravitational signals. *Icarus*, 239:260–272.
- Liu, J., Schneider, T., and Kaspi, Y. (2013). Predictions of thermal and gravitational signals of Jupiter’s deep zonal winds. *Icarus*, 224:114–125. under revision.
- Marotzke, J., Giering, R., Zhang, K., Stammer, D., Hill, C., and Lee, T. (1999). Construction of the adjoint MIT ocean general circulation model and application to Atlantic heat transport sensitivity. *J. Geophys. Res. - Oceans*, 104(C12):29529–29547.
- Mazloff, M. R., Heimbach, P., and Wunsch, C. (2010). An eddy-permitting southern ocean state estimate. *J. Phys. Oceanogr.*, 40:880–899.
- Moore, A. M., Arango, H. G., Broquet, G., Powell, B. S., Weaver, A. T., and Zavala-Garay, J. (2011). The regional ocean modeling system (ROMS) 4-dimensional variational data assimilation systems . part I - system overview and formulation. *Prog. Oceanogr.*, 91:34–49.
- Parisi, M., Galanti, E., Finocchiaro, S., Iess, L., and Kaspi, Y. (2016). Probing the atmospheric dynamics of Jupiter’s Great Red Spot with the Juno gravity experiment. *Icarus*, in press.
- Pedlosky, J. (1987). *Geophysical Fluid Dynamics*. Springer.
- Porco, C. C., West, R. A., McEwen, A., Del Genio, A. D., Ingersoll, A. P., Thomas, P., Squyres, S., Dones, L., Murray, C. D., Johnson, T. V., Burns, J. A., Brahic, A., Neukum, G., Veverka, J., Barbara, J. M., Denk, T., Evans, M., Ferrier, J. J., Geissler, P., Helfenstein, P., Roatsch, T., Throop, H., Tiscareno, M., and Vasavada, A. R. (2003). Cassini imaging of Jupiter’s atmosphere, satellites and rings. *Science*, 299:1541–1547.
- Sanchez-Lavega, A., Hueso, R., and Perez-Hoyos, S. (2007). The three-dimensional structure of saturn’s equatorial jet at cloud level. *Icarus*, 187(2):510 – 519.
- Sanchez-Lavega, A., Rojas, J. F., and Sada, P. V. (2000). Saturn’s zonal winds at cloud level. *Icarus*, 147:405–420.
- Schneider, T. and Liu, J. (2009). Formation of jets and equatorial superrotation on Jupiter. *J. Atmos. Sci.*, 66:579–601.
- Scott, R. K. and Polvani, L. M. (2007). Forced-dissipative shallow-water turbulence on the sphere and the atmospheric circulation of the giant planets. *J. Atmos. Sci.*, 64:3158–3176.
- Showman, A. P., Gierasch, P. J., and Lian, Y. (2006). Deep zonal winds can result from shallow driving in a giant-planet atmosphere. *Icarus*, 182:513–526.
- Sirkes, Z. and Tziperman, E. (1997). Finite difference of adjoint or adjoint of finite difference? *Monthly Weather Review*, 125(12):3373–3378.

- Thacker, W. and Long, R. (1988). Fitting Dynamics To Ddata. *J. Geophys. Res. - Oceans*, 93(C2):1227–1240.
- Tziperman, E. (1992). Computing the steady oceanic circulation using an optimization approach. *Dyn. Atmos. Oceans*, 16:379–403.
- Tziperman, E. and Thacker, W. C. (1989). An optimal-control/adjoint-equations approach to studying the oceanic general circulation. *J. Phys. Oceanogr.*, 19:1471–1485.
- Vasavada, A. R. and Showman, A. P. (2005). Jovian atmospheric dynamics: An update after Galileo and Cassini. *Reports of Progress in Physics*, 68:1935–1996.
- Williams, G. P. (1978). Planetary circulations: 1. barotropic representation of the Jovian and terrestrial turbulence. *J. Atmos. Sci.*, 35:1399–1426.
- Wisdom, J. and Hubbard, W. (2016). Differential Rotation in Jupiter: a comparison of Methods. *Icarus*, *submitted*.
- Wunsch, C. and Heimbach, P. (2007). Practical global oceanic state estimation. *Physica D Nonlinear Phenomena*, 230:197–208.
- Zhang, K., Kong, D., and Schubert, G. (2015). Thermal-gravitational wind equation for the wind-induced gravitational signature of giant gaseous planets: mathematical derivation, numerical method, and illustrative solutions. *Astrophys. J.*, 806(2).
- Zharkov, V. N. and Trubitsyn, V. P. (1978). *Physics of planetary interiors*. pp. 388. Pachart Publishing House.